Nanocrystal fluorescence in photonic bandgap microcavities and plasmonic nanoantennas

Nanocrystal fluorescence in photonic bandgap microcavities and plasmonic nanoantennas

Svetlana G. Lukishova[1], Justin M. Winkler[2], Dilyana Mihaylova[1], Andreas Liapis[3], Luke J. Bissell[4], , David Goldberg[5], Vinod M. Menon[5], Zhimin Shi[6], Robert W. Boyd[1,2,7], Guanuing Chen[8], Paras Prasad[8]

[1]The Institute of Optics, University of Rochester, Rochester, NY 14627, USA
[2]Department of Physics and Astronomy, University of Rochester, Rochester, NY 14627, USA
[3]Brookhaven National Laboratory, Upton, NY 11973, USA
[4]Air Force Research Laboratory, Wright-Patterson Air Force Base, OH 45433, USA
[5]Department of Physics, the City College of New York, New York, NY 10031, USA
[6]Department of Physics, University of South Florida, Tampa, FL 33620, USA
[7]Department of Physics and School of Electrical Engineering and Computer Science, University of Ottawa, Ottawa, Ontario K1N 6N5, Canada
[8]Institute for Lasers, Photonics and Biophotonics and Department of Chemistry, University at Buffalo, USA, Buffalo NY 14260, USA

E-mail: sluk@lle.rochester.edu

Abstract. Results are presented here towards robust room-temperature single-photon sources based on fluorescence in nanocrystals: colloidal quantum dots, color-center diamonds and doped with trivalent rare-earth ions (TR3+). We used cholesteric chiral photonic bandgap and Bragg-reflector microcavities for single emitter fluorescence enhancement. We also developed plasmonic bowtie nanoantennas and 2D-Si-photonic bandgap microcavities.

1. Introduction

Single-photon sources (SPSs) [1-12], producing nonclassical light, are pivotal components in quantum communication technology. They efficiently produce individual photons separated in time with no chance for overlap of photons (antibunching). For photon antibunching the second order coherence function $g^{(2)}(t) = \frac{< I(t)I(t+\tau) >}{< I(\tau) >^2}$ should have a minimum at interphoton time $t = 0$. If $g^{(2)}(0) <$ 0.5, it indicates the absence of photon pairs. Here $I(t)$ is intensity, t and τ are two moments of time, and averaging is time averaging. For common light sources (bulbs, sun light) and in lasers, multiple (nonseparated) photons cannot be avoided even in very faint sources. Using photons that are all temporally separated, absolutely secure quantum communication will prevent any potential eavesdropper (Eve) from intercepting a message without the receiver noticing. Bits of transferred information are coded in the photon polarization state. If the source emitted more than one photon at a time, it would be possible for Eve to extract one of these photons without disturbing the other photons that would reveal Eve's presence. There exist some schemes with classical sources, e.g., using decoy states to reduce leakage of information to an eavesdropper, but for long distance quantum communication with quantum repeaters single-photon sources are important. Some quantum

computation protocols also require single photons. In addition, single photons are very important in metrology and fundamental physics experiments, such as in interference from uncoupled light sources and entanglement-state generation, in shedding light on wave-particle duality as well as in fundamental issues of quantum measurement and uncertainty.

Furthest in development are SPSs based on heterostructured quantum dots placed into 2D-photonic crystal microcavities or into micropillars. In spite of their many advantages in studying cavity quantum electrodynamics, these SPSs are very expensive in fabrication and require cryogenic temperatures. Therefore, many researchers aim for *room-temperature* SPSs. The most popular single emitters for those are dye molecules, colloidal nanocrystal quantum dots and rods, and various color-centers in nanodiamonds. To enhance the single-photon count rate (the bit rate of future quantum information systems) and improve SPS directionality, coupling efficiency into a fiber system and polarization selectivity, single emitters should be embedded in microcavities, photonic crystals and other micro- or nano-structures (e.g., plasmonic nanoantennas, metamaterials, etc.). In addition, an ideal SPS should afford ease of use in a Space environment for the future global quantum communication network.

It should be noted, that similar nano/microstructures can be also used for compact microlasers and on-chip integrated microlasers. The difference being the concentration of dopant: low dopant concentration for SPSs whereas microlasers require high concentration of the same emitters.

The enhancement of spontaneous emission in microcavities is characterized by the Purcell factor [13,14]. This factor is defined as $F_p = \gamma_c/\gamma_0$, where γ_c and γ_0 are the emitter decay rates with and without a cavity, respectively:

$$F_P = \frac{3Q(\lambda/n)^3}{4\pi^2 V_0}\left(\frac{|\boldsymbol{d}\cdot\boldsymbol{E}(r)|}{|d|\cdot|E(r)|}\right)^2, \quad (1)$$

where Q is the cavity quality factor, λ is the free-space wavelength of light, n is the cavity refractive index, V_0 is the cavity mode volume, d is the emitter dipole moment, and $E(r)$ is the local electric field at the position r of the emitter.

Eq. (1) predicts enhancement or diminishing of F_p, depending on the ratio $Q\lambda^3/(V_0 n^3)$, and on how the incident field is aligned with respect to the dipole moment, d. Because high Q values and mode volumes that are small compared to $(\lambda/n)^3$ are required to obtain $F_p >> 1$, it is challenging to increase γ_c at optical frequencies. In recent years, however, semiconductor processing technology and other innovative procedures have enabled enhanced radiative decay rates in microcavities at visible and IR wavelengths, using both cryogenic and room temperature implementations. In addition to increasing γ_c, another advantage of placing the emitter inside a microcavity is the increased coupling efficiency into a single-mode fiber and the polarization selectivity in certain geometries of microcavities or nanoantennas. Even though the Purcell factor is the standard figure of merit for spontaneous emission rate enhancement, care must be taken when using Eq. (1) to describe emission rate enhancements for plasmonic resonances. In the case of plasmonic nanoantennas, the Purcell factor is useful only as a qualitative design guideline.

The structure of this paper is as follows. Section 2 describes single-photon generation and characterization unit of the Institute of Optics, University of Rochester. In Section 3, our results towards room-temperature single-photon sources based on nanocrystal fluorescence (colloidal quantum dots and trivalent rare-earth ions) in 1-D chiral liquid crystal photonic bandgap structures are presented. Section 4 is devoted to a single-photon source based on a Bragg-reflector microcavity with a defect layer doped with nanocrystal quantum dots. In Section 5, gold bowtie plasmonic nanoantenna arrays and nanocrystal manipulation by an atomic force microscope tip are described. Section 6 contains the results of Si 2D-photonic bandgap structures for 1.5 μm wavelength.

2. Single-Photon Generation and Characterization Unit

Figure 1 shows general schematic of experimental set up for single photon generation, detection and characterization. A single-photon generation unit consists of a confocal fluorescence microscope with a high numerical aperture (N.A.) objective that focuses a pulsed or cw-laser beam on a cover glass slip with a single-emitter in a microcavity. The sample is placed on a microscope table located on a piezo-translation stage for a raster scan of the sample around a focused laser beam. Fluorescence light is collected by the same objective. A dichroic mirror reflects laser light and transmits fluorescence light. Interference filters with 6-9 orders of magnitude attenuation further reject an excitation laser light. Single-photon detection and characterization unit represents a Hanbury Brown and Twiss intensity interferometer (correlator), which consists of a nonpolarizing beamsplitter, two single-photon counting, thermoelectrically cooled avalanche photodiode modules (APDs), and start-stop electronics to measure time intervals between two consecutive photons in pairs to prove photon antibunching. The characterization unit also contains electronics and software for confocal fluorescence imaging of single emitters. To increase confocal fluorescence imaging contrast, 150-μm detector areas serve as confocal microscope pinholes.

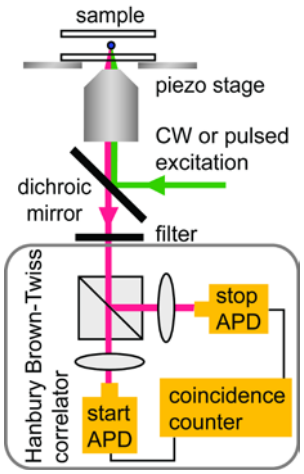

Figure 1. Schematic of a single-photon generation, detection and characterization unit (APD – single-photon counting avalanche photodiode module). A Hanbury Brown and Twiss correlator is used for photon antibunching measurements.

In our experiments we used a home-built confocal fluorescence microscope based on a Nikon TE2000-U inverted microscope with several output ports for diagnostics. We excite our samples with several laser sources: 76 MHz repetition rate, 6 ps pulse duration, 532-nm light from a Lynx mode-locked laser (Time-Bandwidth Products Inc.); 633-nm cw He-Ne laser; 976-nm diode laser; 514 nm cw argon ion laser. Two Si APDs SPCM AQR-14 (Perkin Elmer) were used as a single-photon counting detectors. The time intervals between two consecutively detected photons in separate arms of a Hanbury Brown and Twiss interferometer were measured by a TimeHarp 200 time correlated single-photon counting card with start and stop inputs. A low-light-level, electron-multiplying (EM), thermoelectrically cooled CCD-camera iXon DV 887 ECS-BV (Andor Technologies) was used both for spectral measurements with a Princeton Instruments (SpectraPro2150i) spectrometer, and for wide-field imaging of single-emitter fluorescence. Circular polarization measurements were accomplished using an achromatic quarter-wave plate and linear polarizer. Our polarization data were calibrated for the effect of the optical system on circularly-polarized light. We also performed a radiometric calibration of the optical system, including the spectrometer grating reflectivity dependence on polarization.

3. 1-D Photonic Bandgap Cholesteric Liquid Crystal Structures

Planar-aligned cholesteric liquid crystal (CLC) structures exhibit a chiral 1-D photonic bandgap for the handedness of circularly-polarized light where the electric field vector follows the rotation of the CLC molecular director. Circular polarization with the opposite handedness does not "see" a bandgap and propagates as in an isotropic medium. The stop band is centered at wavelength $\lambda_o = p(n_e + n_o)/2$, where p is the pitch of the CLC spiral structure, and n_e and n_o are extraordinary and ordinary refractive indexes. The bandwidth of the transmission stop band is given by $\Delta\lambda \sim p(n_e - n_o)$. Lasing in such CLC structures occurs at a band edge of this stop band [15-17]. In a similar way, to enhance single-emitter fluorescence in such a microcavity, the single-emitter fluorescence maximum should correspond to a band edge of a CLC structure stop band.

We prepared resonant planar-aligned cholesteric structures for single emitters with fluorescence in visible and near-IR. We used both (1) cholesteric oligomeric powders and (2) monomeric nematic fluids with chiral additives [18-29]. Prepared samples were analyzed using our homemade confocal

microscope setup (Figure 1). By placing an achromatic quarter waveplate and linear polarizer in front of the spectrometer, we were able to filter for right handedness (RH) and left handedness (LH) of circularly polarized (CP) fluorescence.

3.1. Nanocrystal quantum dots in chiral photonic bandgap microcavities

Figure 2 shows our results on circularly polarized microcavity resonance in colloidal nanocrystal quantum dot (NQD) fluorescence doped in a CLC photonic bandgap microcavity [24]. We used left-handed cyclosiloxane oligomeric CLC powder from Wacker Chemie and produced a planar-aligned glassy CLC structure doped with CdSeTe NQD, Qdot 800 ITK organic, Invitrogen, with fluorescence maximum at 790 nm.

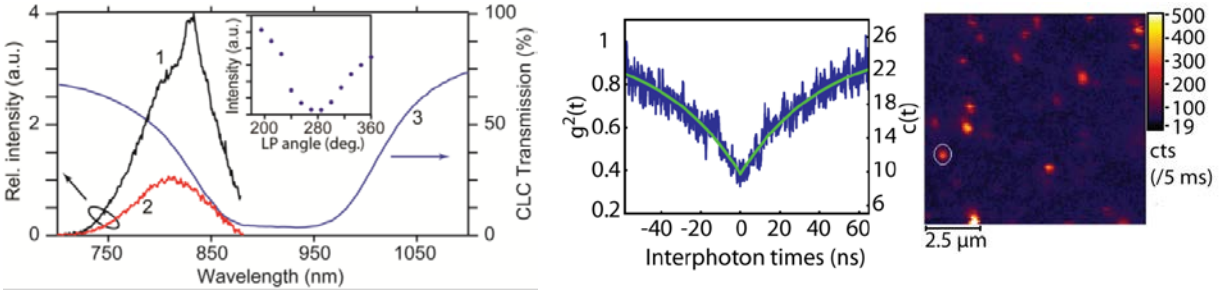

LEFT: **Figure 2**. Circularly-polarized fluorescence resonance from nanocrystal quantum dots (NQDs) doped in a glassy CLC microcavity (633-nm, cw laser excitation). Curve 1: LHCP fluorescence spectrum of the NQDs with a resonance at 833 nm. Curve 2: RHCP fluorescence spectrum for the same NQDs. Curve 3: selective transmission of LHCP light through CLC microcavity. Inset: Dependence of resonance peak intensity on rotation of a linear polarizer (LP) after a fixed quarter wave plate. CENTER and RIGHT: **Figure 3**. Center: Raw coincidence counts *c(t)* (right-hand scale) and $g^{(2)}(t)$ (left-hand scale), showing antibunching (dip at $t = 0$). Right: Confocal fluorescence microscopy image of single CdSeTe NQDs in a glassy CLC photonic bandgap microcavity.

The resulting fluorescence spectra can be seen in Figure 2. LHCP light experienced the photonic bandgap and therefore the black LHCP curve in Figure 2 (curve 1) shows the microcavity resonance, indicating that the LHCP light coupled to the cavity mode. The LHCP fluorescence had a center wavelength of 833 nm and a FWHM of 16 nm ($Q \sim 50$), as compared to a FWHM of 76 nm for RHCP fluorescence. The center wavelength of this resonance roughly matches the edge of the photonic stop band, centered at 910 nm, and shown in Figure 2 by the blue curve 3. The observed RHCP fluorescence is shown in red in Figure 2 (curve 2) and was less intense due to not experiencing the CLC microcavity, showing no sign of line narrowing. The maximum intensity ratio between LHCP and RHCP was a factor of 4.9 [24]. Figure 3, left shows antibunching with $g^{(2)}(0) = 0.382$ of CdSeTe NQD fluorescence under 633 nm laser excitation in a similar glassy CLC photonic bandgap microcavity at lower concentration of NQDs than in the sample of Figure 2. A white circle in Figure 3, right marks a fluorescence image of a single NQD used for antibunching measurements. We also observed antibunching from NV color-center nanodiamonds in a monomeric (fluid) CLC chiral photonic bandgap microcavity [8, 25].

3.2. Rare-earth-doped nanocrystals in chiral photonic bandgap microcavity

A monomeric CLC microcavity made from a mixture of E7 and CB 15 was doped with rare-earth Er^{3+} and Yb^{3+} ions in 20 nm to 30 nm sized $NaYF_4$ nanocrystals with 20% Yb and 2% Er. When these ions were excited using a cw, 976 nm diode laser at incident powers of ~500 µW, we were able to observe upconverted fluorescence of Er^{3+} in visible, as shown in Figure 4, left (red solid curve). The blue dashed curve shows the spectral transmission of this CLC microcavity, measured with unpolarized light.

Energy levels of Er^{3+} and Yb^{3+} and the upconversion excitation scheme under 980 nm excitation are shown in Figure 4, right. The emission lines observed were attributed to the transitions $^2H_{11/2}$, $^4S_{3/2}$

$\rightarrow {}^4I_{15/2}$ (green) and ${}^4F_{9/2} \rightarrow {}^4I_{15/2}$ (red) of the Er^{3+} ions. The populations of upper levels in Er^{3+}occur due to an efficient energy transfer from the Yb^{3+} to the Er^{3+}. This fluorescence was measured to have a circular polarization at 680 nm. It should be noted that Er^{3+} ions also have a fluorescence line at ~1.5 μm, which is important for fiber optical communication.

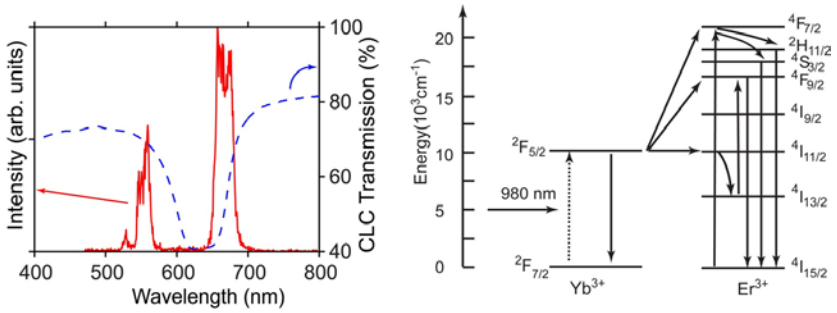

Figure 4. Left: Red solid lines: Fluorescence spectrum of Er^{3+} ions doped in $NaYF_4$ nanocrystals dispersed in a chiral CLC microcavity (E7 and CB15). The blue dashed curve shows the spectral transmission of a CLC microcavity measured with an unpolarized light. Right: Energy levels of Er^{3+} and Yb^{3+} and the upconversion excitation scheme under 980 nm excitation [see Z. Wang et al., Solid State Commun. 144, 255-258 (2007)].

4. Bragg Reflector Microcavity with a Defect Layer Doped with Nanocrystal Quantum Dots

We fabricated a 1-D photonic-bandgap microcavity consisting of a layer of colloidal CdSe/ZnS (core/shell) NQDs spin-cast between two distributed-Bragg reflector (DBR) mirrors (see Figure 5, left) [31]. The DBR mirrors, comprised of alternating layers of SiO_2 (n_{SiO2} ~ 1.54) and SiN_x (n_{SiNx} ~ 2.02).

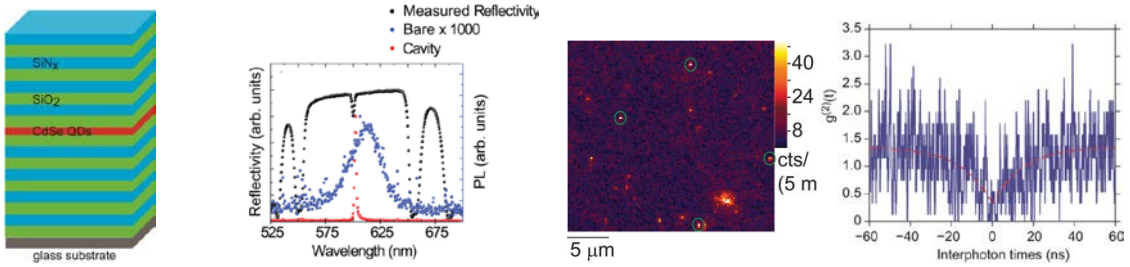

Figure 5. Left: Schematics of a Bragg-reflector microcavity with a defect layer with single NQDs. Center, left: Cavity reflectivity (black curve), fluorescence spectra from NQDs without a microcavity (blue curve) and between two Bragg mirrors (narrow red curve). Center, right: Confocal microscope fluorescence images of several single NQDs (white circles) in a Bragg-reflector microcavity. Right: Coincidence count histogram from single NQDs within the cavity, indicating photon antibunching.

We made two such DBR microcavities with NQD-doped defect layers, using high concentration (~ 1 μM) doping (sample 1), and low-concentration (~ 1 nM) doping (sample 2). Figure 5 (center, black curve) shows the measured reflectivity spectrum of sample 1, with a cavity mode at 600 nm. Figure 5 (center, blue curve) shows the NQD fluorescence spectrum without the second DBR mirror. Figure 5 (center, red curve) shows the spectrum of the NQDs in the DBR microcavity, indicating coupling to the cavity mode, with Q ~ 300. Figure 5 (center) shows confocal microscope fluorescence image of NQDs in a sample 2 under 532 nm laser excitation. For further details of the experimental setup, see Ref. [8]. Figure 5, right, shows the sum of the coincidence count histograms of six NQDs (some of them are marked by the white circles in Figure 5, center). The dip in the histogram at $t = 0$ indicates photon antibunching.

5. Plasmonic Nanoantennas for Single-Photon Source Applications

Using high-precision electron-beam lithography, we fabricated gold bowtie nanoantennas (Figure 6, left). Figure 6, center and right shows our results in antenna polarization selectivity. Figure 7, left shows confocal microscope fluorescence image of NQDs spin-coated on a cover glass slip with gold bowtie nanoantenna arrays. A photoluminescence from gold nano-antenna (periodic array in Figure 7, left) is weak in comparison with NQDs fluorescence. Some NQDs are located within the gaps of nanoantennas (e.g., marked with the stars). Figure 7, right shows fluorescence antibunching curve of one of these NQDs within a bowtie nanoantenna. The second dot fluorescence also reveals antibunching.

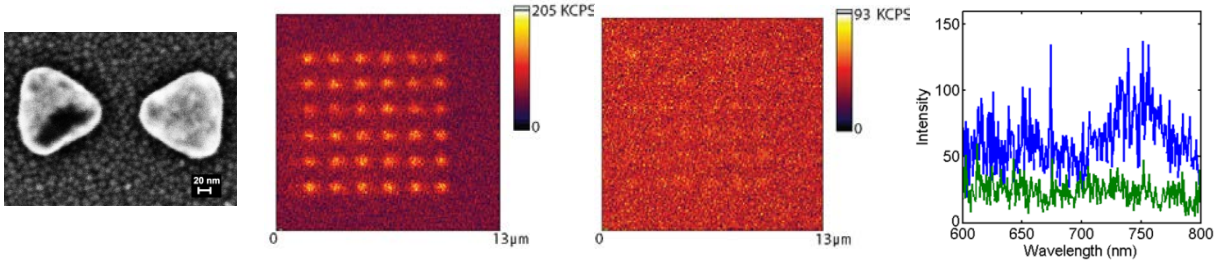

Figure 6. Left: Scanning electron micrograph of a lithographically defined gold bowtie nanoantenna structure with a 60-nm gap. Center: Confocal fluorescence microscope micrographs of gold bowtie nanoantenna array (30-nm-bowtie-gap) for polarization parallel to the bowtie axis (left) and perpendicular to it (right) under 633 nm laser excitation. Right: Photoluminescence spectra from a single gold bowtie nanoantenna under 532 nm laser excitation. The two curves show orthogonal photoluminescence polarizations.

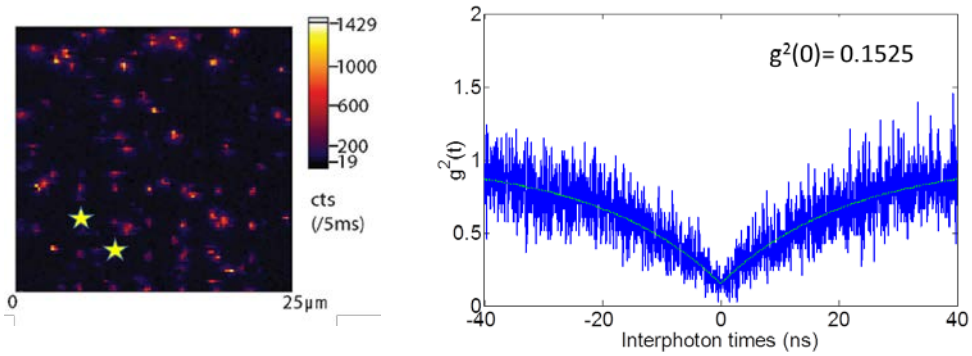

Figure 7. Left: Confocal microscope image of fluorescence from NQDs spin-coated on a cover slip with a bowtie nanoantenna array (633 nm, cw-laser excitation). Right: Fluorescence antibunching of NQD within a gap of a bowtie nanoantenna.

To place 40-50-nm-size nanodiamonds in the gap between the two triangular arms of this nanoantenna we employed a technique to manipulate nanodiamonds using an atomic force microscope (AFM) tip (lithography option of an AFM). Figure 8 shows obtained AFM-micrographs of the nanodiamond manipulation on a spin coated sample by an AFM tip ("pushing" the nanodiamonds). The positions of two nanodiamonds in the three top micrographs are indicated by 1 and 2. The two other micrographs of Figure 8 show nanodiamonds rearranged by an AFM tip to resemble a smiling face. Our next step will be to use this technique to place NV, SiV or Cr-center nanodiamonds or nanocrystals doped with TR3+ in a gap between the arms of the nanoantenna to enhance the photon count rate and directionality, diminish the fluorescence decay time, and provide polarization selectivity.

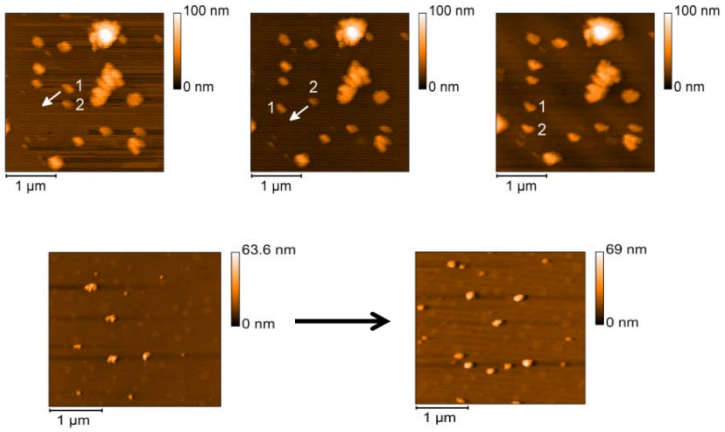

Figure 8. Top: Three AFM micrographs showing the manipulation of nanodiamond position using the AFM tip to "push" the nanodiamonds. Bottom: Two AFM micrographs showing rearrangement of the nanodiamonds by the AFM tip to resemble a smiling face.

6. 2D-Photonic Bandgap Microcavities

Using electron-beam lithography and reactive ion etching we prepared silicon 2D-photonic crystals (PhCs) with L3 defect nanocavities operating at optical communications wavelength around 1.55 μm (see Figure 9, left and center). This L3 nanocavity consists of a triangular lattice of air holes on a silicon membrane, with a line of three holes omitted.

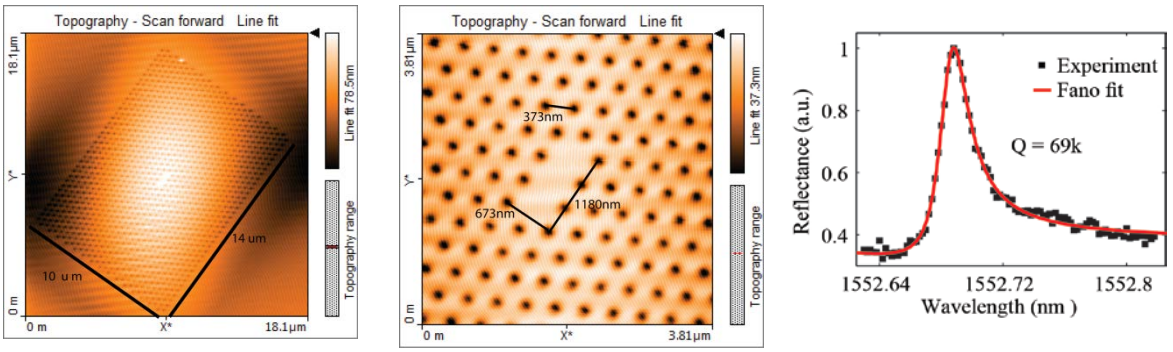

Figure 9. Left and Center: AFM micrographs with different scan area of the same 2D-PhC with a L3 nanocavity. Right: Nanocavity resonance at wavelength near 1.55 µm.

The holes with three slightly different diameters for the same PhC were fabricated on a commercial silicon-on-insulator wafer (SOITEC). The cavity's terminating holes were reduced in size and slightly displaced to increase the cavity Q-factor up to 70,000. Additionally, the radii of selected holes surrounding the cavity were slightly increased to modify the cavity's far-field emission pattern, and facilitate coupling in the out-of-plane direction. Figure 9, right, shows a measured resonance in a typical L3 PhC nanocavity at 1.55 µm wavelength. It should be mentioned that for a similar type of a nanocavity in GaAs with epitaxial quantum dots, a Purcell factor of 145 was reported in Ref. [32]. We are planning to use L3 PhCs with Er^{3+} doped nanocrystals to diminish fluorescence decay times of Er^{3+} fluorescence to a nanosecond range. The nanocavity's rectangular geometry will also provide polarization selectivity.

7. Conclusion

In summary, our results represent progress toward robust and efficient room-temperature SPSs based on fluorescence in nanocrystals. For different applications requiring different wavelengths, we considered colloidal nanocrystal quantum dots (NQDs), color-center nanodiamonds, and nanocrystals doped with trivalent rare-earth ions (TR^{3+}). For single-photon fluorescence control, we used cholesteric chiral photonic bandgap and Bragg-reflector microcavities, developed gold plasmonic bowtie nanoantennas, and Si 2D-photonic-crystal 3L nanocavity. Our next step will be placing a color-center nanodiamond and, separately, a single TR^{3+}-doped nanocrystal between nanoantenna lobes or within a 2D-photonic-crystal 3L-nanocavity to enhance the photon count rate and directionality, reduce the fluorescence decay time for TR^{3+} to tens of nanoseconds, and provide linear polarization selectivity with photon antibunching from nanocrystal within a nanoantenna or nanocavity.

Such SPSs will find applications both in free space and fiber-based quantum cryptography. Some quantum computation protocols also require single photons. In addition, single photons are very important in metrology and fundamental physics experiments, for instance, in interference from uncoupled light sources and entanglement-state generation, in shedding light on wave-particle duality as well as in fundamental issues of quantum measurement and uncertainty.

Acknowledgement

We thank Carlos Stroud and Ansgar Schmid for valuable discussions. Nanoantennas were prepared using the Cornell NanoScale Science & Technology Facility and the University of Rochester Integrated Nanosystems Center. S.G.L. was supported by the U.S. Army Research Office Award DAAD19-02-1-0285, National Science Foundation Awards ECS-0420888, DUE-0633621, DUE-0920500, EEC-1343673. J.M.W. is supported by a NASA Space Technology Research Fellowship NNX11AM82H. L.J.B. was supported by an Air Force SMART Fellowship. R.W.B was supported by the US Defense Threat Reduction Agency—Joint Science and Technology Office for Chemical and Biological Defense (Grant No. HDTRA1-10-1-0025) and by the Canada Excellence Research Chairs Program.

References

[1] Eisaman, M.D., Fan, J., Migdall, A. and Polyakov, S.V., "Invited Review Article: Single-photon sources and detectors", Rev. Scient. Instr. 82, 071101-1-25 (2011).

[2] Yamamoto, Y., Santori, C., Solomon, G., Vuckovic, J., Fattal, D., Waks, E., Diamanti, E., "Single photons for quantum information systems", Progress in Informatics, No 1, 5-37 (2005).

[3] Buckley, S., Kelley Rivoire, K., and Vuckovic, J., "Engineered quantum dot single-photon sources", Rep. Prog. Phys. 75, 126503-1-27 (2012).

[4] Lounis, B., and Orrit, M., "Single-photon sources", Rep. Prog. Phys. 68, 1129 (2005).

[5] Oxborrow, M. and Sinclair, A.G., "Single-photon sources", Contemp. Phys. 46, 173 (2005).

[6] Sheel, S., "Single-photon sources: an introduction", J. Mod. Opt. 56, 141 (2009).

[7] De Vittorio, M., Pisanello, F., Martiradonna, L., Qualtieri, A., Stomeo, T., Bramati, A., Cingolani, R., "Recent advances on single photon sources based on single colloidal nanocrystals", Opto-Electron. Rev. (Springer), 18(1), 1-9 (2010).

[8] Bissell, L.J., [Experimental Realization of Efficient, Room-Temperature Single-Photon Sources with Definite Circular and Linear Polarizations], Ph.D. Thesis, University of Rochester, Rochester, NY (2011).

[9] Lukishova, S.G., "Single-photon sources for secure quantum communication", Proceed. SPIE 9065, paper 90650C (2013).

[10] Santori, C., Fattal, D. and Yamamoto, Y., [Single-photon Devices and Applications], Wiley, Weinheim (2010).

[11] Michler, P., Ed., [Single Semiconductor Quantum Dots], Springer, Berlin (2010).

[12] S.G. Lukishova, J. Winkler, Luke J. Bissell, D. Mihaylova, A.C. Liapis, Z. Shi, D. Goldberg, V.M. Menon, R. Boyd, G. Chen. P.N. Prasad,**"**Room-temperature single photon sources based on nanocrystals in photonic/plasmonic nanostructures", Proceedings SPIE, Emerging Technologies in Security and Defence II; and Quantum-Physics-based Information Security III. Vol. 9254, paper 9254-05, doi: 10.1117/12.2066979 (October 2014).

[13] Novotny, L. and Hecht, B., [Principles of Nano-Optics], Cambridge University Press, Cambridge, New York (2012).

[14] Purcell, E.M., "Spontaneous emission at radio frequencies," Phys. Rev. 69, 681 (1946).

[15] Kopp, V.I., Fan, B., Vithana, H.K.M., Genack, A.Z., "Low-threshold lasing at the edge of a photonic stop band in cholesteric liquid crystals", Opt. Lett. 23, 1707–9 (1998).

[16] Wei, S.K.H., Chen, S.H., Dolgaleva, K., Lukishova, S.G., Boyd, R.W., "Robust organic lasers comprising glassy-cholesteric pentafluorene doped with a red-emitting oligofluorene", Appl. Phys. Lett. 94, 041111 (2009).

[17] Dolgaleva, K., Wei, S.K.H., Lukishova, S.G., Chen, S.H., Schwertz, K., and Boyd, R.W., "Enhanced laser performance of cholesteric liquid crystals doped with oligofluorene dye", J. Opt. Soc. Am. B 25, 1496-1504 (2008).

[18] Lukishova, S.G., Boyd, R.W., Stroud, C.R., "Efficient room-temperature source of polarized single photons", US Patent 7,253,871, Aug. 7, 2007.

[19] Lukishova, S.G., Schmid, A.W., McNamara, A.J., Boyd, R.W., and Stroud, C.R., "Room temperature single photon source: single dye molecule fluorescence in liquid crystal host", IEEE J. Sel. Top. Quant. Electron. 9, No 6, 1512-1518 (2003).

[20] Lukishova, S.G., Schmid, A.W., Supranowitz, C.M., Lippa, N., McNamara, A.J., Boyd, R.W., Stroud, C.R., "Dye-doped cholesteric-liquid-crystal room-temperature single photon source ", J. Mod. Opt. 51, No 9-10, 1535 -1547 (2004).

[21] Lukishova, S.G., Schmid, A.W., Knox, R.P., Freivald, P., McNamara, A., Boyd, R.W., Stroud, C.R., Marshall, K.L., "Single-photon source for quantum information based on single dye molecule fluorescence in liquid crystal host", Molec. Cryst. Liq. Cryst. 454, 403-416 (1-14) (2006).

[22] Lukishova, S.G., Bissell, L.J., Menon, V.M., Valappil, N., Hahn, M.A., Evans, C.M., Zimmerman, B., Krauss, T.D., Stroud, C.R., Boyd, R.W., "Organic photonic bandgap microcavities doped with semiconductor nanocrystals for room-temperature on demand single photon sources", J. Mod. Opt. 56, is 2 & 3, 167-174 (2009).

[23] Lukishova, S.G., Bissell, L.J., Stroud, C.R., Boyd, R.W., "Room-temperature single photon sources with definite circular and linear polarizations", Opt. and Spectr. 108, No 3, 417-424 (2010).

[24] Lukishova, S.G., Bissell, L.J., Winkler, J., and Stroud, C.R., "Resonance in quantum dot fluorescence in a photonic bandgap liquid crystal host", Opt. Lett. 37, Issue 7, 1259-1261 (2012).

[25] Lukishova, S.G., "Liquid crystals under two extremes: (1) high-power laser irradiation, and (2) single-photon level", Mol. Cryst. Liq. Cryst. 559, 127-157 (2012).

[26] Lukishova, S.G., Schmid, A.W., "Near-field optical microscopy of defects in cholesteric oligomeric liquid crystal films", Molec. Cryst. Liq. Cryst. 454, 15-21 (2006).

[27] Lukishova, S.G., Schmid, A.W., Knox, R., Freivald, P., Bissell, L., Boyd, R.W., Stroud, C.R., Marshall, K.L., "Room temperature source of single photons with definite polarization", J. Mod. Opt. 54, iss. 2 & 3, 417-429 (2007).

[28] Winkler, J.M., Lukishova, S.G., Bissell, L.J., Goldberg, D., Menon, V.M., Shi, Z., Boyd, R.W., "Room-temperature single photon sources: nanocrystals in photonic bandgap microcavities and plasmonic nanoantennae," Single Photon Workshop, Book of Abstracts, Oak Ridge National Laboratory, Oak Ridge, TN (October 2013).

[29] Lukishova, S.G., Liapis, A.C., Bissell, L.J., Gehring, G.M., and Boyd**,** R.W., "Single-photon experiments with liquid crystals for quantum science and quantum engineering applications", Liquid Crystal Reviews 2, No. 2, 111–129 (2014).

[30] Lukishova, S.," Efficient single-photon sources with definite polarization", 1 October 2014, SPIE Newsroom. DOI: 10.1117/2.1201409.005604.

[31] Goldberg, D. and Menon, V.M., "Enhanced amplified spontaneous emission from colloidal quantum dots in all-dielectric monolotic microcavities", Appl. Phys. Lett., 102, 081119 (2013).

[32] Hennessy, K, Badolato, A., Winger, M., Gerace, D., Atature, M., Gulde, S., Falt, S., Hu, E.L., Imamoglu, A., "Quantum nature of a strongly coupled single quantum dot-cavity system", Nature 445, 896-899 (2007).